Split-HaloTag® Imaging Assay for Sophisticated Microscopy of Protein-Protein Interactions *in planta*

Rieke Minner-Meinen[1], Jan-Niklas Weber[1], Andreas Albrecht[2], Rainer Matis[2], Maria Behnecke[1], Cindy Tietge[1], Stefan Frank[1], Jutta Schulze[1], Henrik Buschmann[3], Peter Jomo Walla[2], Ralf-R. Mendel[1], Robert Hänsch[1,4]* and David Kaufholdt[1]

r.meinen@tu-bs.de, jan-niklas.weber@tu-bs.de, andreas.albrecht@tu-bs.de, r.matis@tu-bs.de, maria.behnecke@dsmz.de, cindy.oettel@tu-bs.de, stefan.frank@tu-bs.de, jutta.schulze@tu-bs.de, Henrik.buschmann@biologie.uni-osnabrueck.de, p.walla@tu-bs.de, r.mendel@tu-bs.de, r.haensch@tu-bs.de, d.kaufholdt@tu-bs.de

[1]Institut für Pflanzenbiologie, Technische Universität Braunschweig, Humboldtstrasse 1, D-38106 Braunschweig, Germany

[2]Institut für Physikalische und Theoretische Chemie, Technische Universität Braunschweig, Hagenring 30.023c, D-38106 Braunschweig, Germany

[3]Botany Department, Universität Osnabrück, Barbara Str. 11, 49076 Osnabrück Germany

[4]Center of Molecular Ecophysiology (CMEP), College of Resources and Environment, Southwest University, Tiansheng Road No. 2, 400715 Chongqing, Beibei District, P.R. China

*author for correspondence: Tel: +49-(0)531-391-5867
Fax: +49-(0)531-391-8128
E-Mail: r.haensch@tu-bs.de

Date of submission: 2020-10-29

Word count total: 5370

Number of Tables: 0

Number of Supplementary Tables: 2

Number of Figures: 4

Number of Supplementary Figures: 0

Running title: Split-HaloTag® Imaging Assay

Abstract

An ever-increasing number of protein complexes participating in metabolic pathways and of multi-protein intracellular networks have been identified in plant cells. Split-GFP based protein-protein interaction assays combine the advantages of *in vivo* interaction studies in a native environment with additional visualisation of protein complex localisation. However, fluorescence proteins entail several drawbacks for sophisticated microscopy: high photobleaching rate during long-term observations, correlation of fluorescence intensity to expression level or blinking behaviour. With the HaloTag® system these drawbacks can be overcome asthis reporter is able to form covalent irreversible bonds with several synthetic photostable fluorescence ligands,which can be used in variable concentrations for optimal fluorescence intensity. Therefore, we established the new Split-HaloTag® imaging assay to enable sophisticated fluorescence imaging of protein-protein interactions. This is demonstrated using an well-characterised interaction as an example for protein-protein interaction at cellular structures: the molybdenum cofactor biosynthesis complex anchoring to filamentous actin. Additionally, a specific interaction was visualised with advanced subdiffractional polarisation microscopy in a more distinctive manner as example for sophisticated imaging. Therefore, this assay is a promising new tool for continuative 3D-imaging, single molecule tracking and super-resolution microscopy of protein-protein interactions in plant cells.

Keywords

advanced microscopy, cytoskeleton, photostable fluorescence dyes, Gateway cloning, Molybdenum cofactor biosynthesis complex, polarisation microscopy, protein-protein interaction, Split-HaloTag® imaging assay

Abbreviations

BiFC: bimolecular fluorescence complementation; diAcFAM: diacetyl derivative of fluorescein; FP: fluorescence protein; SPoD: Super-resolution by polarisation demodulation; TMR: Tetramethylrhodamine

55 **Introduction**

56 Understanding the cellular biology of plants requires the characterisation of protein-protein
57 interactions. An increasing number of protein networks and substrate channeling pathways
58 have been identified (Zitnik *et al*., 2019). The bimolecular fluorescence complementation
59 (BiFC) , as one of many protein fragment complementation assays, is one of the most popular
60 and frequently used methods for plants to study protein-protein interactions. It allows
61 visualisation and localisation of protein interactions in living cells (Bhat *et al*., 2006). Non-
62 fluorescent reporter fragments are fused genetically to putative interaction partners and an
63 interaction between the two allows formation of a bimolecular fluorescent complex
64 (Kerppola, 2008). The advantage of using fluorescent proteins (FP) is a fluorescence signal
65 without an invasive insertion of a chemical compound into the cell. However, some drawbacks
66 of FPs can severely hamper microscopic analysis: a direct interlink between fluorescence
67 intensity and fusion construct expression level, low quantum efficiency, blinking behaviour, a
68 high photobleaching rate during long-term observations (Reck-Petersen *et al.*, 2006),
69 photoswitching (Morisaki and McNally, 2014) as well as the tendency of FPs to form oligomers
70 (Miyawaki *et al*., 2003). These drawbacks are especially unfavourable when using
71 sophisticated fluorescence imaging methods such as two-photon, single molecule,
72 subdiffractional polarisation or super-resolution imaging. These methods typically require
73 fluorescence dyes of high stability and brightness (Moerner and Kador, 1989; Orrit and
74 Bernard, 1990; Bode *et al*., 2008; Holleboom *et al*., 2014; Liao *et al*., 2010/2011; Godin *et al*.,
75 2014; Loison *et al*., 2018; Camacho *et al*., 2019).

76 However, self-labelling enzyme tags such as the HaloTag® have been shown to overcome
77 these drawbacks of FPs and are suitable for such microscopy methods and super-resolution
78 imaging (Grimm *et al*., 2015; Lee *et al*., 2010). The HaloTag® System (Promega,
79 https://www.promega.de/) is based on the bacterial haloalkane dehalogenase DhaA (EC
80 3.8.1.5) from *Rhodococcus rhodochrous* (Liss *et al*., 2015). The tag was modified to form
81 covalent irreversible bonds with synthetic chloralkane ligands (Los *et al*., 2008; England *et al.,*
82 2015). This covalent bond is formed rapidly under physiological environments and remains
83 intact even under stringent conditions (Los and Wood, 2007). Numerous ligands are available
84 for the HaloTag® including different fluorescent dyes with extended spectral range,
85 photostability and membrane permeability such as the red fluorescent rhodamine derivative

86 TMR (tetramethylrhodamine), the green fluorescent Oregon Green or the yellow fluorescent
87 diacetyl derivative of fluorescein DiAcFAM. Furthermore, dyes can be varied in their dosages
88 to either label all or only a few molecules which is needed for single-molecule tracking
89 approaches. In addition, HaloTag® proteins keep their monomeric structure, so the tag will
90 not lead to oligomerisation of protein fusion partners (Banaz *et al*., 2018). The usability of this
91 imaging system was shown successfully *in planta* (Lang *et al.,* 2006)

92 In 2012, Ishikawa and colleagues identified several split points within the HaloTag® protein
93 and demonstrated its reconstitution ability. These results gave rise to the idea of establishing
94 the Split-HaloTag® imaging assay *in planta.* This new approach is particularly useful for
95 characterising protein complex assembly at structural elements including cell membranes or
96 the cytoskeleton. The possibility of using these microscopy techniques will enable to study
97 local formation and dynamics of a given complex with improved details compared to BiFC and
98 conventional confocal laser scanning microscopy. Single-molecule tracking approaches with
99 limited fluorescent dye will enable the tracing of complex mobility at the cytoskeleton or
100 inside the membrane system. In this study, we used the previously described anchoring of the
101 molybdenum cofactor biosynthesis complex via molybdenum insertase Cnx1 to filamentous
102 actin (Kaufholdt *et al*., 2017) for establishing of the new Split-HaloTag® imaging assay. In this
103 way, we demonstrate the advantages of this assay for imaging of *in vivo* protein-protein
104 interactions via advanced microscopy.

105 Material and Methods

106 Cloning of Split-HaloTag® Gateway destination vectors

107 The optimised HaloTag®-7 sequence (298 amino acids) from Promega
108 (https://www.promega.de/) was genetically split on position 155/156 aa into the N-terminal
109 fragment "NHalo" (aa 1-155) and the C-terminal fragment "CHalo" (aa 156-298) according to
110 the initial experiment of Ischikawa and colleagues (2012). In order to create Split-HaloTag®
111 GATEWAY® destination vectors, enabling C-terminal Split-HaloTag® reporter fusion, the binary
112 destination vectors pDest- *Cluc*-GW and pDest-GW-*Cluc* were used (Gehl *et al.,* 2011). PCR-
113 Primers were designed to fuse specific restriction enzyme recognition sequences at both
114 reporter fragments (Table S1). After amplification, *Cluc* fragments were exchanged by
115 restriction and ligation for *Nhalo* or *Chalo* residues using the restriction sites *Xba*I and *Spe*I (N-

116 terminal) and *Xho*I/*Sac*I (C-terminal), respectively (restriction enzymes purchased by Thermo
117 Fischer Scientific (https://www.thermofisher.com)), to create pDest-*Nhalo*-GW, pDest-*GW-*
118 *Nhalo,* pDest-*Chalo*-GW and pDest-*GW-Chalo* (Table S2).

119 **Expression vectors**

120 Coding sequences of Cnx6 (AT2G43760), Cnx7 (AT4G10100) and Map65 (amino acids 340–
121 587; AT5G55230) were fused to Split-HaloTag® fragments via a two-step fusion PCR with
122 Phusion-Polymerase purchased from Thermo Fischer Scientific
123 (https://www.thermofisher.com). For the first PCR, each single cDNA and reporter fragment
124 was created with an overlapping sequence to each, which enable assembly of fusion
125 constructs (used primers listed in Table S1). For the second step, the products of the first PCR
126 were assembled due to the overlapping matching sequences and then amplified a one single
127 fragment. This *att*B-site flanked constructs were subcloned via BP-reaction into the Donor
128 vector pDONR/Zeo to create entry vectors. Recombining these into pK7WG2 (Karimi *et al*.,
129 2002) using LR-reactions generated the expression vectors pExp-*Nhalo-cnx7*, pExp-*Chalo- cnx6*
130 and pExp-*Chalo-map65.*

131 All BiFC expression vectors and entry vectors with coding sequences of Cnx1 (AT5G20990), LA
132 (Lifeact; amino acids 1–17 of the *Saccharomyces cerevisiae* protein ABP140), ABD2
133 (aminoacids 325–687; AT4G26700), CKL6 (amino acids 302–479; AT4G28540) and NLuc were
134 available and are described by Kaufholdt *et al*. (2016a). The entry vectors were used to clone
135 Split-HaloTag® expression vectors via LR-reactions into pDest-*GW-Nhalo* and pDest-*GW-Chalo*
136 to create pExp-*cnx1-Nhalo,* pExp-*la-Nhalo,* pExp-*ckl6-Nhalo,* pExp-*la-Chalo,* pExp-*abd2-Chalo*
137 and pExp-*Nluc-Chalo.*

138 **Plant transformation**

139 *N. benthamiana* wild type plants were cultivated in soil under greenhouse conditions. They
140 were used for *Agrobacterium*-mediated transient transformation of fusion constructs 7 to 12
141 weeks after germination as described by Gehl and colleagues (2011). *Agrobacterium* strain
142 C58C1/pMP90 carrying binary expression vectors were freshly grown (48 h at 28 °C) on solid
143 CPY media (0.1% (w/v) yeast extract, 0.5% (w/v) casein peptone, 0.5% (w/v) sucrose, 2 mg/L
144 $MgSO_4$ x $7H_2O$ (pH 7); 1.5% w/v agar) containing rifampicin (50 mg/L) and gentamycin

145 (50 mg/L) as well as kanamycin (50 mg/L). Helper strain p19 (Voinnet *et al.*,2003) was grown
146 on CPY medium containing rifampicin (50 mg/L) and kanamycin (50 mg/L). After growing for
147 20 h in 9 mL of liquid CPY at 200 rpm at 28 °C, cells transferred into fresh activation medium
148 (10 mM MES/KOH (pH 5.6), 10 mM $MgCl_2$,150 µM acetosyringone). Before infiltration of the
149 bacteria into the leaves, each strain was diluted in activation media to an optical density of
150 OD_{600} = 0.9 (final OD_{600} = 0.3). Then, three strains were mixed for each transformation: (i) One
151 strain containing a NHalo construct, (ii) one strain containing a CHalo-construct and (iii) the
152 helper strain p19. After incubation for 2 h at 50 rpm (28 °C), mixed *Agrobacterium* suspension
153 were infiltrated into abaxial site of young but fully expanded leaves. Plants were incubated for
154 3-5 days in the green house.

155 **Staining of *N. benthamiana* leaves discs with HaloTag® ligands**

156 Staining protocol was based on the work of Lang and colleagues (2006). Leaf discs of (6-
157 10 mm) of *N. benthamiana* leaves were transferred into a 20 mL syringe with screw lid and
158 infiltrated with 2-4 mL ligand solution (0.5, 1.0 or 2.0 µM TMR, DiAcFAM and Oregon Green in
159 10 mM MES/KOH (pH 5.6) and 10 mM $MgCl_2$). All dyes were purchased from Promega
160 (https://www.promega.de/). Syringes with leaf discs were wrapped in aluminium foil and
161 incubated for 0.5, 15, 30 or 60 min either on the work bench, on a tumbling shaker or on a
162 rotary tube mixer. After staining, the samples were washed with 10 mL washing solution by
163 closing the screw lid and moving the plunger up and down for 10 times. Washing steps were
164 repeated with fresh washing solution 6-12 times. Furthermore, one duration before the last
165 washing step of 0, 3 or 12 hours in washing solution was performed.

166 **Confocal laser scanning microscopy**

167 The confocal Laser Scanning Microscope LSM 510Meta from Zeiss (Göttingen, Germany) was
168 used. The cLSM-510META scanhead was connected to the Axiovert 200M. All images were
169 examined using either the Plan-Neofluar 10x/0.3 or the C-Apochromat 40x/1.2 water-
170 immersion objective. For excitation, both an argon laser (488 nm for BiFC, Oregon Green and
171 DiAcFAM as well as chlorophyll fluorescence) and a Helium-Neon Laser (543 nm line for TMR)
172 was used. The emitted light passed the primary beam-splitting mirror UV/488/543/633 and
173 was separated by a secondary beam splitter at 545 nm. Fluorescence was detected with filter
174 sets as follows: BP 505-530 nm for BiFC (Em_{max}: 515 nm), Oregon Green (Em_{max}: 520 nm) and

175 DiAcFAM (Em_{max}: 521 nm); BP 560-615 for TMR (Em_{max}: 578 nm); LP 650 nm for chlorophyll
176 fluorescence. Bright field images were taken with the transmitted light photomultiplier. All
177 images were taken using ZEISS Microscope Software ZEN 2009 and processed with ZEN lite
178 and Fiji (Schindelin *et al*., 2012). The shown images depict represented cells of several
179 analysed leaves from at least three independent transformations.

180 **Super-resolution by polarisation demodulation microscopy**

181 Principles of the experimental set-up are described by Hafi and colleagues (2014) and
182 modifications enabling the analysis of the dye´s 3D-orientations were described by Albrecht
183 *et al*. (2020). The cover slip was fixed to the microscope slide with nail polish. Linearly polarised
184 light deriving from a 488 nm continuous wave (CW) laser (sapphire 488-50, Coherent) was
185 used for excitation of Oregon Green molecules. The beam was expanded through a telescope
186 system. The polarisation was modulated at 15 frames per modulation period by rotation of a
187 λ/2-waveplate. The rotation was achieved through a chopper wheel (Optical Chopper
188 Systems, Thorlabs) which was synchronised to an electron-multiplying charge-coupled device
189 (EMCCD) camera (iXonEM+897 back illuminated, Andor Technology). Through the rotation of
190 2 wedge prisms lateral shift of the beam was caused that enabled measurements of the
191 fluorophores being excited from a different direction. Then, the beam was focused onto the
192 back aperture of the microscope objective (UPlanSApo, 60×, NA = 1.35 oil immersion,
193 Olympus), which was integrated in an inverted microscope body (IX 71, Olympus). Emitted
194 light was then passed through a dichroic mirror (beam splitter z 488 RDC, AHF) and an emission
195 filter (ET band pass 525/50, AHF). To further magnify the image and focus it the EMCCD
196 camera an additional lenses system was used. During the measurement 2,000 frames at
197 approximately 32 ms per frame were recorded. The first 200 frames were neglected for
198 calibration purposes. The raw fluorescence intensity of all modulation periods of the last 1,800
199 frames of a measurement was used for analyses. Images were "deblurred" by using
200 deconvolution algorithms. The "blurring" function or point-spread function (PSF) was
201 approximated by using the PSF-Generator Plugin for ImageJ
202 (http://bigwww.epfl.ch/algorithms/psfgenerator/). Using the PSF, the modulating
203 fluorescence intensities were deblurred using an iterative least-squares deconvolution while
204 accounting for the polarisation modulation. The least-squares functional was minimised by
205 using the FISTA Algorithm (Beck and Teboulle, 2009).

206 ## Results and Discussion

207 The Split-HaloTag® constructs created in this study are based on the enhanced HaloTag®-7
208 sequence (298 amino acids), which has been optimised and improved with regard to solubility,
209 stability, binding kinetics and access to an optional TEV-cleavage site (Ohana *et al*., 2009). It
210 was split on position 155/156 aa into the N-terminal fragment "NHalo" (aa 1-155) and the C-
211 terminal fragment "CHalo" according to the initial experiment of Ischikawa and colleagues
212 (2012). The two amino acids important for covalent ligand binding are located on each of the
213 two separate Split-HaloTag® fragments. The stable bond between HaloTag® protein and ligand
214 is formed by the catalytic amino acid Asp^{106} as part of the "NHalo" fragment. In the mutated
215 HaloTag® protein the substituted Asn^{272} (HaloTag®-7) as part of "CHalo" traps the reaction
216 intermediate as a stable covalent adduct. Therefore, independent expression of "NHalo" or
217 "CHalo" fragments will not enable ligand binding without each other (Fig. 1A/B), which is a
218 fundamental aspect when using Split-HaloTag® imaging for investigation of protein-protein
219 interactions. The cDNAs of the interaction partners were fused N- or C-terminally to the NHalo
220 and CHalo fragments via fusion PCR and gateway cloning (see Materials and Methods). For
221 high flexibility, Split-HaloTag® GATEWAY compatible destination vectors were generated
222 which enabled a fast and easy cloning of expression vectors with coding sequences of different
223 proteins of interest.

224 **Reconstitution of Split-HaloTag® *in planta***

225 The complex formation of the heterotetrameric molybdopterin synthase (MPT) subunits Cnx6
226 and Cnx7 from *Arabidopsis thaliana* was used to demonstrate the capability of reconstitution
227 of the Split-HaloTag® *in planta*. This protein pair was chosen as positive control due to their
228 verified high binding strength (Kaufholdt *et al*., 2013). The two interacting proteins (Fig. 1C)
229 will bring the two HaloTag® reporter fragments in close spatial proximity and, thereby, guide
230 the reconstitution of functional HaloTag® proteins.

231 After transformation of *Nicotiana benthamiana* epidermis cells and staining with the
232 fluorescent ligand TMR, specific cytoplasmic fluorescence was observed as a thin layer at the
233 cell periphery (Fig. 1D). Wild type leaves were stained similarly, and lacking fluorescence
234 signals indicated the washing steps being sufficient to remove unbound ligands (Fig. 1E).
235 Therefore, since the MPT synthase complex is localised in the cytoplasm, HaloTag® fragments

236 CHalo and NHalo were capable of reconstitution reconstitution guided by the strong
237 interaction of Cnx6 and Cnx7. After proving the general reconstitution, this new assay was
238 tested in a second approach including proteins attached to cytoskeleton structures such as
239 filamentous (F-) actin as well as microtubules. By applying this approach, it was possible to
240 test whether the Split-HaloTag® system allows for investigating the assembly of different
241 proteins at cytoskeletal elements. Both structures were not labelled directly to NHalo or CHalo
242 termini, but via binding proteins, as a fusion of larger reporter fragments directly to globular
243 actin or tubulin proteins might disturb their polymerisation processes. For F-actin labelling,
244 the binding domain of fimbrin from *A. thaliana* (ABD2; Sheahan *et al*., 2004) as well as of
245 Abp140 from *Saccharomyces cerevisiae* (Lifeact/LA; Riedl *et al*., 2008) were used.
246 Furthermore, microtubule binding domains of the two proteins Casein-Kinase-1-Like-6 (CKL6;
247 Ben-Nissan *et al*., 2008) and the Microtubule Associated Protein 65 (Map65; Hamada, 2007)
248 from *A. thaliana* were investigated. The cytoskeleton binding proteins show no direct protein
249 interactions to each other. However, their affinity and subsequent binding and anchoring to
250 the cytoskeletal structures results in such spatial proximity that it is able to act as model for a
251 direct interaction of a cytoskeleton associated protein complex (Kaufholdt *et al*., 2016a).

252 Expression of F-actin binding protein constructs followed by HaloTag® reconstitution and
253 staining resulted in a TMR specific fluorescence visible as transversely arranged filaments with
254 branches distributed throughout the cytoplasm (Fig. 1F). The approach with CLK6-NHalo and
255 CHalo-Map65 to label microtubules upon Split-HaloTag® reconstitution displayed filamentous
256 structures more equally distributed throughout the cell with less cross bridges compared to
257 actin filaments (Fig. 1G). These structures are typical for F-actin and microtubules,
258 respectively, which were observed in BiFC experiments before. In all interaction approaches
259 both actin filaments as well as microtubules, could successfully be visualised upon interaction
260 of cytoskeletal binding proteins. It has to be noted that staining and washing procedure can
261 cause severe stress and damage to the cells. In addition to the orange fluorescent ligand TMR
262 (Em_{max} 578 nm), the ligands Oregon Green (Em_{max} 520 nm) as well as DiAcFAM (Em_{max}
263 526 nm) were tested as all three dyes are cell-permeant and suitable for intracellular labelling
264 (Promega). As expected, also Oregon Green and DiAcFAM (data not shown) were able to bind
265 reconstituted HaloTag®. This demonstrates a general binding capability of the reconstituted
266 HaloTag® exemplary for a plurality of other available dyes depending on the individual setting.

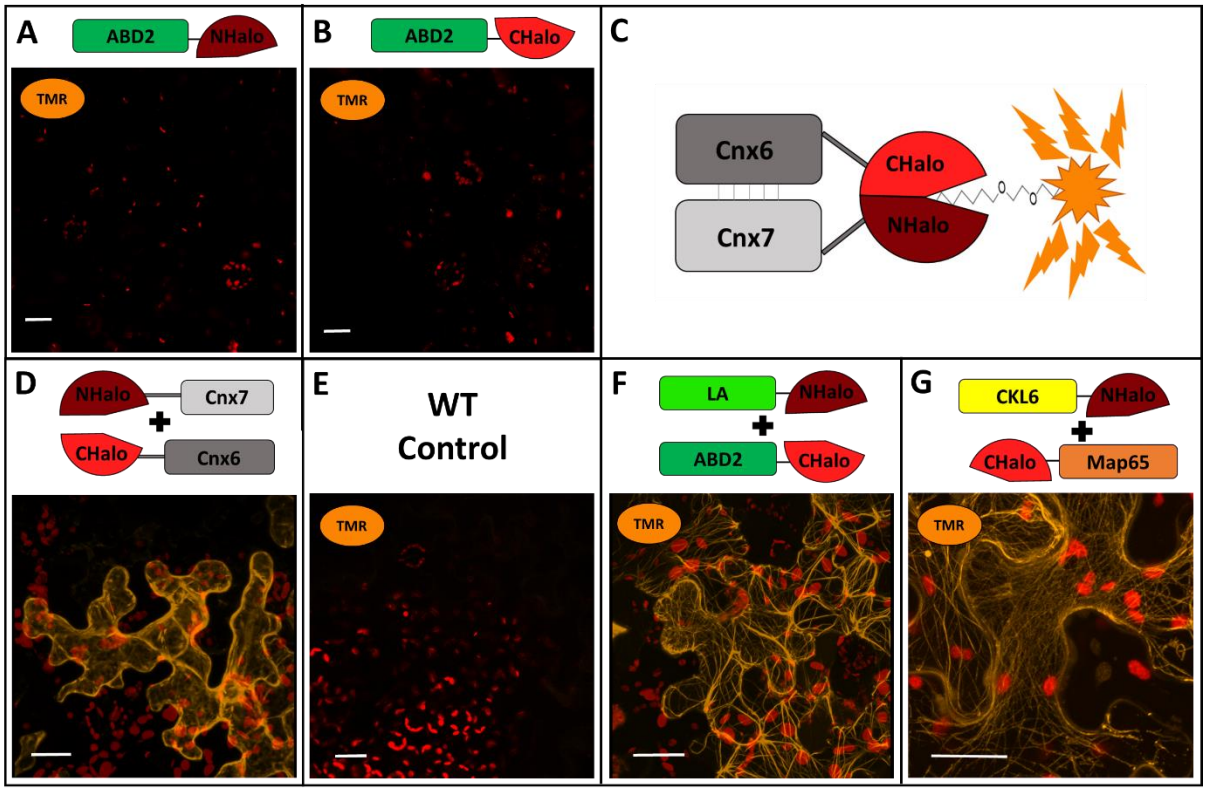

Fig. 1: Testing Split-HaloTag® complementation upon protein interactions of MPT synthase complex as well as at cytoskeleton binding proteins.

Shown are images of *N. benthamiana* epidermis cells via confocal microscopy detecting TMR. Staining of leaf discs was performed 4-5 days after transformation. All images were taken with a C-Apochromat 40x/1.2 water immersion objective. Scale bars depict a length of 20 µm each. **(A/B)** Negative controls of single transformed Split-HaloTag® reporter constructs fused to ABD2. **(C)** Schematic illustration of Split-HaloTag® reconstitution guided by the MPT synthase subunits Cnx6 and Cnx7 **(D)** Cytosolic TMR fluorescence after transformation with NHalo-Cnx7 and Cnx6-CHalo. **(E)** Negative control of a wildtype (WT) leaf after staining. **(F)** TMR fluorescence at actin after transformation of actin binding constructs LA-NHalo and ABD2-CHalo. **(G)** TMR fluorescence at microtubules filaments after transformation of microtubules binding constructs CKL6-NHalo and CHalo-Map65.

Insights into the Staining Protocol

It has been described by Lang and colleagues (2006), who first introduced the HaloTag® system to plant cells, that especially destaining procedures are of great importance to reduce unspecific background fluorescence. For interaction studies, comparison of fluorescence intensity and fluorescence pattern is the main task, where each form of background will falsify the result. However, after using the published destaining protocol an excess of unbound dye remained in the tissue. Therefore, optimised staining and destaining procedures had to be

286 established. To improve staining protocols and to evaluate the best HaloTag® ligand several
287 different factors were investigated: (i) the size of analysed leaf discs (6; 8; 10 & 12 cm in
288 diameter), (ii) concentration of ligands (0.5, 1 & 2 µM), (iii) ligand incubation time (1 min up
289 to 1 h), (iv) number of subsequent washing steps (6 up to 12),, (v) incubation time in washing
290 solution (3 h up to 12 h) and (vi) aeration of leaf discs in washing solution.

291 During this optimisation process, several general observations were made. After TMR staining,
292 fluorescence was always detected in vascular tissue of transformed as well as wild type leaves
293 suggesting a nonspecific adhesion between TMR and molecules in leaf veins (Fig. 2A).
294 Furthermore, staining with more than 0.5 µM TMR combined with an insufficient number of
295 washing steps resulted in oversaturation and accumulation of unbound dye in the cytoplasm
296 of parenchyma cells (Fig. 2B). This amount of unbound TMR accumulation increased when
297 using larger or damaged leaf discs or older plants. Moreover, recycling of frozen TMR solution
298 led to unspecific aggregations inside the cells.

299 DiAcFAM staining gained an overall weaker fluorescence signal compared to TMR but no
300 staining of vascular tissue was observed (not shown). However, weak DiAcFAM signals (Em_{max}
301 521 nm) could easily be mistaken for typical plant background fluorescence at approx.
302 530 nm. Furthermore, accumulation of unbound ligands occurred especially in stomata after
303 DiAcFAM (Fig. 2C) but also after Oregon Green (Fig. 2D) staining. In addition, Oregon Green
304 resulted in accumulation inside vacuoles of parenchyma cells if incubated more than a few
305 seconds in staining solution (Fig. 2E).

306 After testing of the different staining parametersoptimal results for TMR staining were
307 obtained using leaf discs of a diameter of 6-8 mm, a final TMR concentration of 0.5 µM in 2 mL
308 fresh staining solution, 15 min incubation time and followed by eight subsequent washing
309 steps into a 20 mL syringe and an overnight incubation in washing solution. Samples were
310 incubated with 10 mL washing solution by closing the screw lid and moving the plunger up
311 and down for approx. 10 times. Immediately before microscope analysis two more washing
312 steps were performed. Both, overnight incubations either on a tumbling shaker or on a rotary
313 tube mixer were equally sufficient for all dyes, as long as there was sufficient air in the syringe
314 to allow leaf disc aeration.

315 Oregon Green showed optimal results if a 0.5 µM staining solution was exchanged with 2 mL
316 washing solution immediately after its infiltration and incubated for 15 minutes. Then, the
317 washing procedure was applied as described for TMR. This could reduce but not completely
318 avoid Oregon Green accumulation.

319 Overall, all exemplary tested dyes are suitable for intracellular labelling of HaloTag® proteins
320 in plant tissue, which leads to the assumption that other HaloTag® ligands will be suitable for
321 other experimental settings as well. From all three tested dyes, TMR was the brightest,
322 showing the least drawbacks. However, even after prolonged overnight incubation in
323 repeatedly refreshed washing solution TMR was still bound to vascular tissue. Therefore, leaf
324 area further away from vascular tissue should be used for analysis. In this study, both TMR
325 and Oregon Green showed ideal properties for confocal laser scanning microscopy despite
326 Oregon Green accumulations. Due to a different experimental set-up only Oregon Green was
327 used in SPoD microscopy. TMR showed the best applicability for usage within a Split-HaloTag®
328 complementation assay for staining *N. benthamiana* leaf discs.

329 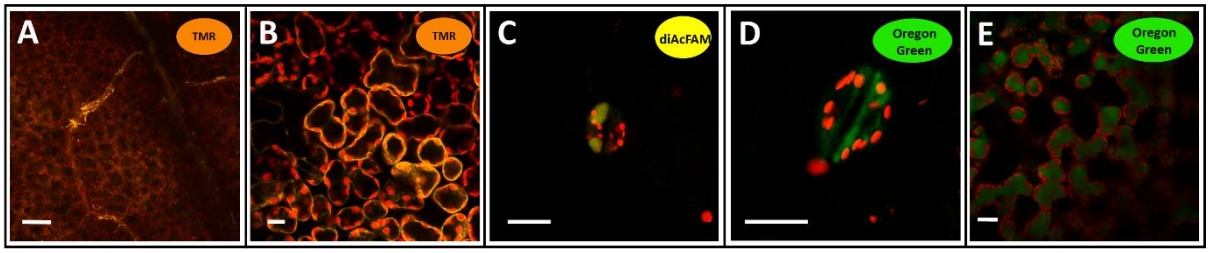

330 **Fig. 2: Evaluation of HaloTag® fluorescent Ligands TMR, DiAcFAM and Oregon Green.**
331 Confocal microscopy of *N. benthamiana* leaf discs stained with TMR **(A/B)**, DiAcFAM **(C)** or Oregon
332 Green **(D/E)**. Images were taken either with a Plan-Neofluar 10x/0.3 **(A)** or with a C-Apochromat
333 40x/1.2 water immersion objective **(B-E)**. Scale bars depict a length of 100 µm **(A)** or 20 µm **(B-E)**. **(A)**
334 Unspecific TMR binding in vascular tissue. **(B)** Oversaturation of unbound TMR in parenchyma cells
335 after using 2 µM dye. **(C/D)** Accumulation of unbound ligands in stomata after DiAcFAM **(C)** and Oregon
336 Green **(D)** staining. **(E)** Accumulation of unbound Oregon Green in parenchyma cells.

337 **Validation of Split-HaloTag® imaging upon protein-protein interaction at actin filaments**

338 After proving the general capability of Split-HaloTag® fragment reconstitution, we aimed at
339 validating this new assay via an binding assay of the molybdenum insertase Cnx1 to F-actin as
340 a well-characterised example for an protein-protein interaction study at cell structures

341 (Kaufholdt *et al*. 2016a).. This established setting via cytoskeleton binding proteins for
342 interaction studies *in vivo* was used to investigate whether the Split-HaloTag® system
343 demonstrate the F-actin binding of Cnx1 in the same manner it was shown by BiFC
344 experiments before. Therefore, *in vivo* protein-protein interaction studies require adequate
345 negative controls as discussed by Kaufholdt *et al*. (2016a) in detail. As negative control protein,
346 the cytosolic protein NLuc (N-terminus of the luciferase from *Photinus pyralis*) was provided,
347 which had no interaction with the analysed proteins of interest (Gehl *et al*., 2011).

348 In the interaction approach, reporter fusion constructs of Cnx1 and the actin binding protein
349 LA, respectively, were co-expressed in *N. benthamiana*. For comparison, the BiFC approach
350 described by Kaufholdt et al. (2016a) was included, for which the reporter halves VYNE (N-
351 terminus of Venus) and SCYCE (C-terminus of SCFP) were used (Gehl *et al*., 2009). Both BiFC
352 and Split-HaloTag® complementation assay show almost identical results (Fig. 3 A/B). Both
353 TMR and GFP fluorescence were detected in a filamentous pattern concentrated at the actin
354 nucleus basket and thinned out at F-actin towards the cellular cortex. A typical pattern for
355 studying an actin interacting protein complex was observed in both approaches that is
356 reminiscent of a "starry sky" (Kaufholdt *et al*., 2016a) caused by F-actin anchoring of the
357 interacting proteins in close proximity to its synthesis by the two actin binding domains of LA
358 and Cxn1. When LA-NHalo was co-expressed with NLuc-CHalo in the negative control, TMR
359 specific fluorescence at actin filaments was detected, too. A background fluorescence was
360 expected caused by reconstitution by chance in the small cytosolic space, which is typical for
361 split-protein assays in plant cells (Gehl *et al*., 2009/2011). A negative control without any
362 fluorescence would be an unrealistic event in plants, which should be verified by an additional
363 abundance control (Kaufholdt *et al*., 2016b). Relating to the background, Split-HaloTag® has
364 the same performance as all known protein-protein interacting studies, however, in the
365 interaction approach stronger fluorescence or different pattern will demonstrate an
366 interaction. The TMR fluorescence was equally distributed within the cell of the negative
367 control and no starry sky could be observed (Fig. 3C). Consequently, identical results of both
368 BiFC and Split-HaloTag® were observed showing the characteristic "starry sky" like pattern
369 demonstrating its interaction with F-actin as it was discussed before by Kaufholdt *et al*.
370 (2016a) This proves exemplary the applicability of the Split-HaloTag® system on the basis of a
371 protein binding to the cytoskeleton.

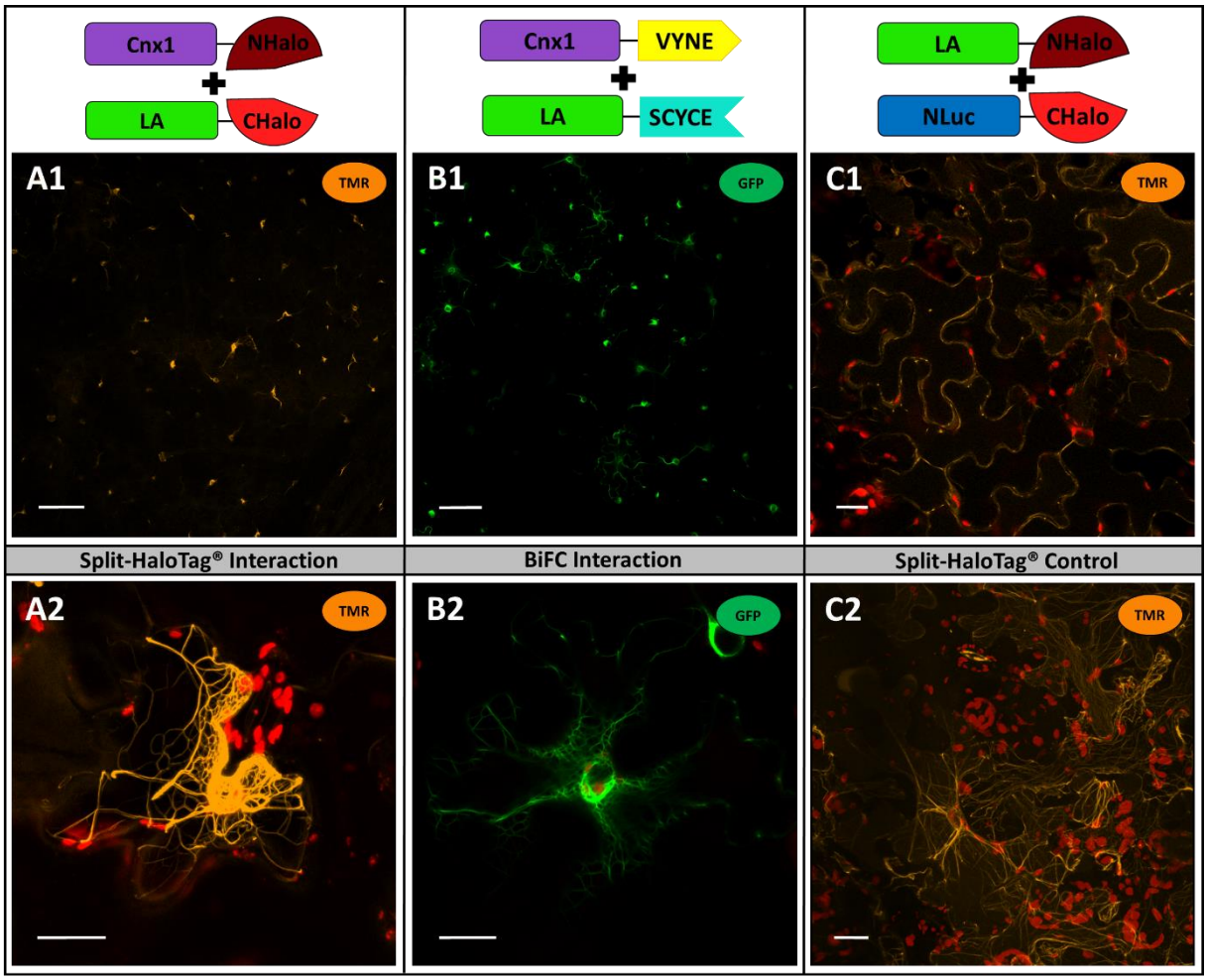

Fig. 3: Split-HaloTag® Protein-Protein Interaction Studies of Cnx1 and Actin Filaments via Lifeact. Shown are images of *N. benthamiana* epidermis cells via confocal microscopy of TMR or GFP. Staining of leaf discs was performed 4-5 days after transformation. All images were taken with a Plan-Neofluar 10x/0.3 **(A1/B1/C1)** or with a C-Apochromat 40x/1.2 water immersion objective **(A2/B2/C2).** Scale bars depict a length of 100 µm **(A1/B1/C1)** or 20 µm **(A2/B2/C2)**. **(A)** Split-HaloTag® approach with Cnx1-NHalo and LA-CHalo. **(B)** BiFC approach with Cnx1-VYNE and LA-SCYCE. **(C)** Corresponding Split-HaloTag® negative control where Cnx1 was replaced by the independent protein NLuc. **(A)** and **(B)** were imaged with identical setting for optimal comparison of strength and pattern.

Application examples of Split-HaloTag® for sophisticated **imaging.**

The Split-HaloTag® imaging assay has been proven as a feasible method for imaging of protein interactions. However, conventional light and fluorescence microscopy are diffraction-limited to a resolution limit of approx. 200 nm in the lateral (x-y) and about 600 nm in the axial (z) direction (Cremer and Masters, 2013). Many subcellular structures are smaller which hampers their detailed observation (Huang *et al.*, 2009). To circumvent these restrictions, advanced

387 fluorescence imaging methods such as single molecule detection, subdiffractional polarisation
388 imaging or super-resolution microscopy (SRM) techniques have been developed to improve
389 the resolution and to allow studying molecular processes more detailed (Moerner and Kador
390 1989; Orrit and Bernard, 1990; Bode *et al*., 2008; Holleboom *et al*., 2014; Liao *et al*.,
391 2010/2011; Godin *et al*., 2014; Loison *et al*., 2018; Camacho *et al*., 2019). However, stable
392 fluorescence dyes emitting light at various wavelength are needed for such advanced imaging
393 techniques, which is hard to realise by standard fluorescence proteins (Banaz *et al*., 2018). The
394 Split-HaloTag® system has the advantage of using such stable dyes flexible on a fusion protein
395 complex. . Liss *et al*. (2015) for example used HaloTag® and a TMR ligand successfully in animal
396 cell cultures for correlative light and electron microscopy (CLEM) of protein dynamics with
397 ultrastructure details. Reck-Peterson and colleagues (2006) used the HaloTag® to label dynein
398 in sea urchin axonemes and tracked single molecules with a precision of a few nanometres to
399 reveal dynein´s stepping behaviour at microtubules. Small organic fluorophores can be used
400 in variable dosages to label only a few molecules and are available with different spectral
401 behavior. Moreover, several organic fluorophores especially for live-cell labelling and
402 subsequent imaging were recently developed with photoactivatable properties (Lee *et al.,*
403 2010) as well as with improved quantum efficiency and superior brightness while retaining
404 excellent cell permeability (Grimm *et al*., 2015).

405 As a first approach, interaction of Cnx1 and the actin binding protein ABD2 were performed
406 to show the resolution potential of stable TMR fluorescence for confocal laser scanning
407 microscopy. For this purpose, each layer of a cell has to be scanned in very thin optical slices
408 (µm range or less). Such a detailed imaging can take several minutes, which leads to high
409 damages through photo bleaching at standard fluorescence proteins. However, the stable
410 TMR fluorescence of a Split-HaloTag® enabled more defined results of cell images (Fig. 4A)
411 compared to BiFC approaches (Fig. 4B), which is demonstrated by the very thin filaments of
412 the actin network hardly detectable by BiFC.

413 Super-resolution by polarisation demodulation (SPoD) microscopy was used as second
414 example for demonstrating the performance of the Split-HaloTag® system. This advanced
415 fluorescence imaging technique is a subdiffractional polarisation imaging method that allows
416 measurement of the average orientation of fluorescent dyes attached to different structures
417 and was first described by Hafi and colleagues (2014). Fluorescent molecules are illuminated

418 via linearly polarised light. This causes the fluorophores to be excited at different times, which
419 results in a modulated fluorescence intensity from the fluorophores. Depending on the
420 orientation of the illuminated fluorophores (or more specifically the orientation of their
421 transition dipole moments), the observed fluorescence intensity will be phase-shifted, and
422 differently oriented fluorophores will emit periodic signals peaking at different points in time.
423 Therefore, the analyses via deconvolution algorithms allow a high resolution imaging of cell
424 structures (for details see Albrecht *et al*., 2020). . During each measurement, 2,000 frames
425 were recorded, which in itself is not problematic when using stable dyes. Split-HaloTag®
426 constructs with the two microtubule binding domains of CLK6 and Map65 were used for this
427 purpose. Overexpression of MAP65 isotypes is known to result in microtubule bundling (Mao
428 *et al*. 2006). After transformation and expression, leaf discs were stained with Oregon Green,
429 which wavelength was more appropriate for SPoD microscopy. The observed fluorescence
430 resulted in individual microtubules (Fig. 4B1). Albeit high amounts of background fluorescence
431 and out-of-focus signal complicated the recording and modulation analysis, subdiffractional
432 separation in a branching region of distinct fibres was observed in the deconvolved image (Fig.
433 4B2) and was supported by different phases as visualised by a simple red/green colour code.
434 These different phases in the branching region of the two fibres were already observable in
435 the raw modulation data. Certainly, future work is needed to enhance separation by different
436 phases in addition to pure image deconvolution for entire cell images. Nevertheless, Split-
437 HaloTag® imaging assay can be used for such advanced fluorescence imaging techniques,
438 which failed in case of BiFC.

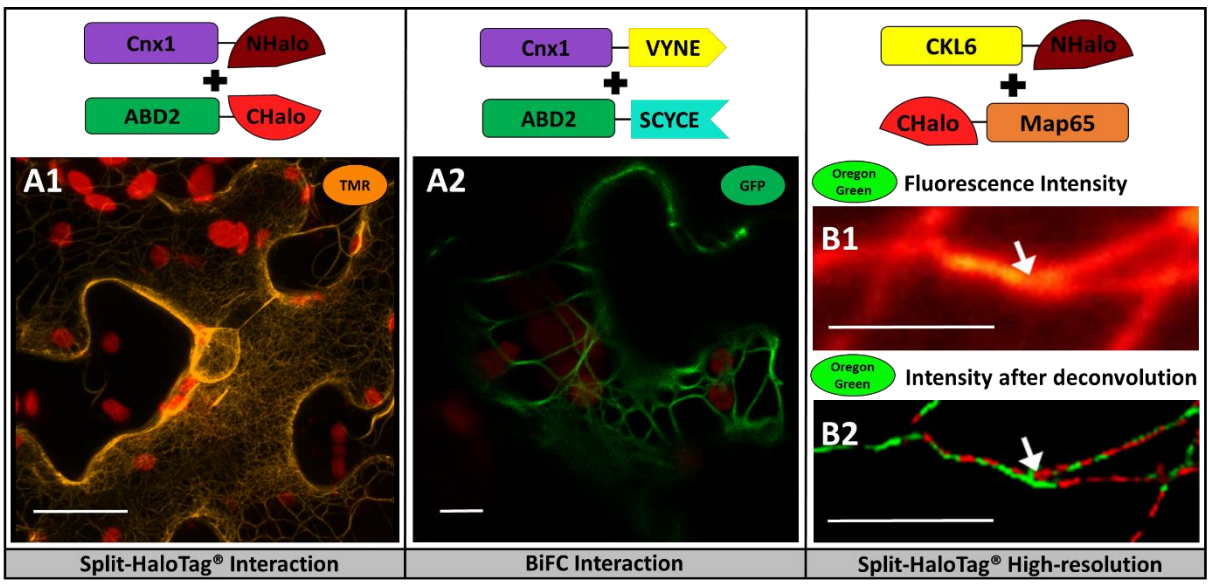

439

440 **Fig. 4: Analysis of Split-HaloTag® images via confocal microscopy and super-resolution SPoD**
441 **microscopy.**
442 Shown are representative *N. benthamiana* cells three days after transformation. **(A)** Interaction studies
443 at actin filaments with Cnx1 and ABD2 via Split-HaloTag® **(A1)** or BiFC **(A2)**. Split-HaloTag® Staining was
444 performed with TMR. Images were taken with a C-Apochromat 40x/1.2 water immersion objective.
445 Scale bars depict a length of 20 µm. **(B)** SPoD microscopy of microtubules stained with Oregon Green
446 after transformation of the Split-HaloTag® microtubules binding constructs CKL6-NHalo and CHalo-
447 Map65. **(B1)** Diffraction limited image depicting averaged raw fluorescence intensity. **(B2)** Phase colour
448 coded fluorescence intensity image after 1000 iterations of the deconvolution algorithm. The
449 red/green colourcode support subdiffractional separation of the fibres at a distinct branching fork
450 (arrow) that is not visible in the conventional diffraction of wide field image. However, future work is
451 needed to enhance separation by different phases in addition to pure image deconvolution for entire
452 cell images. The raw data scale bars depict 2 µm each.

453 ## Conclusion

454 In this study, the Split-HaloTag® imaging assay was established for the first time *in planta*.
455 Vectors were cloned and reporter termini NHalo and CHalo were tested for reconstitution in
456 both fusion orientations to the protein of interest and in all four orientation combinations to
457 each other. The applicability of the system for interaction studies was demonstrated using
458 previously published protein interactions forming the Molybdenum cofactor biosynthesis
459 complex including its anchoring to F-actin. An additional infiltration of a fluorescent ligand into
460 the cell with subsequent washing was a disadvantage compared to BiFC. A reconstitution
461 background by change was observed in all split-protein assays. However, the benefit of the
462 Split-HaloTag® system lies in the ability to visualise specific protein interactions in advanced
463 imaging techniques. Therefore, this system can be used in future for sophisticated imaging
464 techniquessuch as 3D-microscopy, polarisation-microscopy, single-molecule tracking or
465 super-resolution imaging methods that require brighter and more stable fluorescence
466 markers. Localisation of protein complexes can be observed with the split-HaloTag® imaging
467 assay in a distinct manner. In live-cell microscopy, the method combines *in vivo* split-reporter
468 analyses with the previous shown advantages of the HaloTag® like a large set of differently
469 coloured fluorescent ligands, their photostability compared to fluorescence proteins and the
470 ability to vary labelling intensity via dosage of dyes independent from protein expression.

471 Therefore, this assay is a new tool for sophisticated imaging of protein-protein interactions in
472 plant cells.

473 Supplemental information

474 Supplemental data are available online.

475 Table S1: Primers for Cloning and sequencing of Split-HaloTag® related constructs and vectors.

476 Table S2: Split-HaloTag® Destination and Expression vectors used within this work.

477 Acknowledgement

478 We are grateful to Dr. Christin-Kirsty Baillie for scientific support and critical reading. We thank
479 Tanja Linke for excellent technical work in our lab. This work was financially supported by the
480 Deutsche Forschungsgemeinschaft (grant GRK2223/1) to RH and RRM.

481 Author Contribution

482 RMM, HB, PJW, RRM, RH and DK planned and designed the project. RMM, JNW, MB, CT, SF,
483 JS and DK cloned the vectors, performed plant transformation and the cLSM experiments. AA
484 and RM handled SPoD microscopy. All authors analysed and discussed the results. RMM, JNW,
485 RH and DK were primarily involved in drafting the manuscript and RMM and DK produced
486 figures and tables. JS, HR, PJW and RRM critically read the manuscript and improved the text,
487 all authors finalised it. RH and DK coordinated the work.

References

Albrecht, A., Pfennig, D., Nowak, J., Matis, R., Schaks, M., Hafi, N., Rottner, K., Walla, P. J. (2020). Amplitude Analysis of Polarization Modulation Data and 3D-Polarization Demodulation (3D-SPoD). *bioRxiv*. https://doi.org/10.1101/2020.03.10.986034.

Banaz, N., Mäkelä, J., Uphoff, S. (2018). Choosing the right label for single-molecule tracking in live bacteria: side-by-side comparison of photoactivatable fluorescent protein and Halo tag dyes. Journal of physics D: Applied physics, 52(6), 064002.

Beck, A., Teboulle, M. (2009). A fast iterative shrinkage-thresholding algorithm with application to wavelet-based image deblurring. In 2009 IEEE International Conference on Acoustics, Speech and Signal Processing, pp. 693-696.

Ben-Nissan, G., Cui, W., Kim, D. J., Yang, Y., Yoo, B. C., Lee, J. Y. (2008). Arabidopsis casein kinase 1-like 6 contains a microtubule-binding domain and affects the organization of cortical microtubules. Plant physiology, 148(4), 1897-1907.

Bhat, R. A., Lahaye, T., Panstruga, R. (2006). The visible touch: in planta visualization of protein-protein interactions by fluorophore-based methods. Plant methods, 2(1), 12.

Bode, S., Quentmeier, C. C., Liao, P. N., Barros, T., Walla, P. J. (2008). Xanthophyll-cycle dependence of the energy transfer between carotenoid dark states and chlorophylls in NPQ mutants of living plants and in LHC II. Chemical Physics Letters, 450(4-6), 379-385.

Camacho, R., Täuber, D., Scheblykin, I. G. (2019). Fluorescence Anisotropy Reloaded—Emerging Polarization Microscopy Methods for Assessing Chromophores' Organization and Excitation Energy Transfer in Single Molecules, Particles, Films, and Beyond. *Advanced Materials*, *31*(22), 1805671.

Cremer, C., Masters, B. R. (2013). Resolution enhancement techniques in microscopy. The European Physical Journal H, 38(3), 281-344.

England, C. G., Luo, H., Cai, W. (2015). HaloTag technology: a versatile platform for biomedical applications. Bioconjugate chemistry, 26(6), 975-986.

Gehl, C., Waadt, R., Kudla, J., Mendel, R. R., Hänsch, R. (2009). New GATEWAY vectors for high throughput analyses of protein–protein interactions by bimolecular fluorescence complementation. Molecular plant, 2(5), 1051-1058.

516 **Gehl, C., Kaufholdt, D., Hamisch, D., Bikker, R., Kudla, J., Mendel, R. R., Hänsch, R.** (2011).
517 Quantitative analysis of dynamic protein–protein interactions in planta by a floated-leaf luciferase
518 complementation imaging (FLuCI) assay using binary Gateway vectors. The Plant Journal, 67(3), 542-
519 553.

520 **Godin, A. G., Lounis, B., Cognet, L. (**2014). Super-resolution microscopy approaches for live cell
521 imaging. Biophysical journal, 107(8), 1777-1784.

522 **Grimm, J. B., English, B. P., Chen, J., Slaughter, J. P., Zhang, Z., Revyakin, A., Patel, R., Macklin, J. J.,**
523 **Normanno, D., Singer, R. H., Lionnet, T., Lavis, L. D.** (2015). A general method to improve fluorophores
524 for live-cell and single-molecule microscopy. Nature methods, 12(3), 244.

525 **Hafi, N., Grunwald, M., Van Den Heuvel, L. S., Aspelmeier, T., Chen, J. H., Zagrebelsky, M., Schütte,**
526 **O. M., Steinem, C., Korte, M., Munk, A., Walla, P. J.** (2014). Fluorescence nanoscopy by polarization
527 modulation and polarization angle narrowing. Nature methods, 11(5), 579.

528 **Hamada, T.** (2007). Microtubule-associated proteins in higher plants. Journal of plant research, 120(1),
529 79-98.

530 **Holleboom, C. P., Walla, P. J.** (2014). The back and forth of energy transfer between carotenoids and
531 chlorophylls and its role in the regulation of light harvesting. Photosynthesis research, 119(1-2), 215-
532 221.

533 **Huang, B., Bates, M., Zhuang, X.** (2009). Super-resolution fluorescence microscopy. Annual review of
534 biochemistry, 78, 993-1016.

535 **Ishikawa, H., Meng, F., Kondo, N., Iwamoto, A., Matsuda, Z.** (2012). Generation of a dualfunctional
536 split-reporter protein for monitoring membrane fusion using self-associating split GFP. Protein
537 Engineering, Design & Selection, 25(12), 813-820.

538 **Karimi, M., Inzé, D., Depicker, A.** (2002). GATEWAY™ vectors for Agrobacterium-mediated plant
539 transformation. Trends in plant science, 7(5), 193-195.

540 **Kaufholdt, D., Gehl, C., Geisler, M., Jeske, O., Voedisch, S., Ratke, C., Bollhöner, B., Mendel, R. R.,**
541 **Hänsch, R.** (2013). Visualization and quantification of proteininteractions in the biosynthetic pathway
542 of molybdenum cofactor in *Arabidopsis thaliana*. J. Exp. Bot. 64, 2005–2016.

543 **Kaufholdt, D., Baillie, C. K., Bikker, R., Burkart, V., Dudek, C. A., von Pein, L., Rothkegel, M., Mendel,**
544 **R. R., Hänsch, R.** (2016a). The molybdenum cofactor biosynthesis complex interacts with actin
545 filaments via molybdenum insertase Cnx1 as anchor protein in Arabidopsis thaliana. Plant Science, 244,
546 8-18.

547 **Kaufholdt, D., Baillie, C. K., Meyer, M. H., Schwich, O. D., Timmerer, U. L., Tobias, L., van Thiel, D.,**
548 **Hänsch, R. Mendel, R. R.** (2016b). Identification of a protein-protein interaction network downstream
549 of molybdenum cofactor biosynthesis in Arabidopsis thaliana. Journal of plant physiology, 207, 42-50.

550 **Kaufholdt, D., Baillie, C. K., Meinen, R., Mendel, R. R., Hänsch, R.** (2017). The Molybdenum Cofactor
551 Biosynthesis Network: In vivo Protein-Protein Interactions of an Actin Associated Multi-Protein
552 Complex. Frontiers in plant science, 8, 1946.

553 **Kerppola, T. K.** (2013). Bimolecular fluorescence complementation (BiFC) analysis of protein
554 interactions in live cells. Cold Spring Harbor Protocols, 2013(8), pdb-prot076497.

555 **Lang, C., Schulze, J., Mendel, R. R., Hänsch, R. (**2006). HaloTag™: A new versatile reporter gene system
556 in plant cells. Journal of experimental botany, 57(12), 2985-2992.

557 **Lee, H. L. D., Lord, S. J., Iwanaga, S., Zhan, K., Xie, H., Williams, J. C., Wang, H., Bowman, G. R., Goley,**
558 **E. D., Shapiro, L., Twieg, R. J., Rao, J., Moerner, W. E..** (2010). Superresolution imaging of targeted
559 proteins in fixed and living cells using photoactivatable organic fluorophores. Journal of the American
560 Chemical Society, 132(43), 15099-15101.

561 **Liao, P.N., Bode, S., Wilk, L., Hafi, N., Walla, P. J.** (2010). Correlation of electronic carotenoid–
562 chlorophyll interactions and fluorescence quenching with the aggregation of native LHC II and
563 chlorophyll deficient mutants. Chemical Physics, 373(1-2), 50-55.

564 **Liao, P. N., Pillai, S., Gust, D., Moore, T. A., Moore, A. L., Walla, P. J.** (2011). Two-Photon Study on the
565 Electronic Interactions between the First Excited Singlet States in Carotenoid− Tetrapyrrole Dyads. The
566 Journal of Physical Chemistry A, 115(16), 4082-4091.

567 **Liss, V., Barlag, B., Nietschke, M., Hensel, M. (**2015). Self-labelling enzymes as universal tags for
568 fluorescence microscopy, super-resolution microscopy and electron microscopy. Scientific reports, 5,
569 17740.

570 **Loison, O., Weitkunat, M., Kaya-Çopur, A., Alves, C. N., Matzat, T., Spletter, M. L., Luschnig, S.,**
571 **Brasselet, S., Lenne, P. F., Schnorrer, F.** (2018). Polarization-resolved microscopy reveals a muscle

572 myosin motor-independent mechanism of molecular actin ordering during sarcomere maturation.
573 PLoS biology, 16(4), e2004718.

574 **Los, G., Wood, K.** (2007). The HaloTag: A novel technology for cell imaging and protein analysis.
575 Methods. Mol. Biol. 356, 195–208.

576 **Los, G. V., Encell, L. P., McDougall, M. G., Hartzell, D. D., Karassina, N., Zimprich, C., Wood, M. G.,**
577 **Learish, R., Ohana, R. F., Urh, M., Simpson, D., Mendez, J., Zimmermann, K., Otto, P., Vidugiris, G.,**
578 **Zhu, J., Darzins, A., Klaubert, D. H., Bulleit, R. F., Wood, K. V.** (2008). HaloTag: a novel protein labeling
579 technology for cell imaging and protein analysis. ACS chemical biology, 3(6), 373-382.

580 **Mao, G., Buschmann, H., Doonan, J. H., Lloyd, C. W.** (2006). The role of MAP65-1 in microtubule
581 bundling during Zinnia tracheary element formation. Journal of cell science, 119(4), 753-758.

582 **Miyawaki, A., Sawano, A., Kogure, T.** (2003). Lighting up cells: labelling proteins with fluorophores.
583 Nat Cell Biol., S1-S7.

584 **Moerner, W. E., Kador, L.** (1989). Optical detection and spectroscopy of single molecules in a solid.
585 Physical review letters, 62(21), 2535.

586 **Morisaki, T., McNally, J. G.** (2014). Photoswitching-Free FRAP Analysis with a Geneticall Encoded
587 Fluorescent Tag. PLoS ONE, 9(9), e107730

588 **Ohana, R. F., Encell, L. P., Zhao, K., Simpson, D., Slater, M. R., Urh, M., Wood, K. V.** (2009). HaloTag7:
589 a genetically engineered tag that enhances bacterial expression of soluble proteins and improves
590 protein purification. Protein expression and purification, 68(1), 110-120.

591 **Orrit, M., Bernard, J.** (1990). Single pentacene molecules detected by fluorescence excitation in a p-
592 terphenyl crystal. Physical review letters, 65(21), 2716.

593 **Reck-Peterson, S. L., Yildiz, A., Carter, A. P., Gennerich, A., Zhang, N., Vale, R. D.** (2006). Single-
594 molecule analysis of dynein processivity and stepping behavior. Cell, 126(2), 335-348.

595 **Riedl, J., Crevenna, A. H., Kessenbrock, K., Yu J. H., Neukirchen, D., Bista, M., Bradke, F., Jenne, D.,**
596 **Holak, T. A., Werb, Z., Sixt, M., Wedlich-Soldner, R.** (2008). Lifeact: a versatile marker to visualize F-
597 actin. Nature methods, 5(7), 605.

598 **Schindelin, J., Arganda-Carreras, I., Frise, E., Kaynig, V., Longair, M., Pietzsch, T., Preibisch, S.,**
599 **Rueden, C., Saalfeld, S., Schmid, B., Tinevez, J. Y., White, D. J., Hartenstein, V., Eliceiri, K., Tomancak,**

P., Cardona, A. (2012). Fiji: an open-source platform for biological-image analysis. Nature methods, 9(7), 676-682.

Sheahan, M. B., Staiger, C. J., Rose, R. J., & McCurdy, D. W. (2004). A green fluorescent protein fusion to actin-binding domain 2 of Arabidopsis fimbrin highlights new features of a dynamic actin cytoskeleton in live plant cells. Plant physiology, 136(4), 3968-3978.

Voinnet, O., Rivas, S., Mestre, P., Baulcombe, D. (2003). An enhanced transient expression system in plants based on suppression of gene silencing by the p19 protein of tomato bushy stunt virus. Plant J. 33, 949–956.

Zitnik, M., Feldman, M. W., Leskovec, J. (2019). Evolution of resilience in protein interactomes across the tree of life. Proceedings of the National Academy of Sciences, 116(10), 4426-4433